Measurement of the spin correlation parameters A_{ll} and A_{sl} for the reaction $pp \rightarrow d\pi^+$ in the energy region 500–800 MeV

D. B. Barlow,* A. Saha,† and K. K. Seth
Northwestern University, Evanston, Illinois 60201

T. S. Bhatia,‡ G. Glass, J. C. Hiebert, R. A. Kenefick, S. Nath, L. C. Northcliffe, and W. B. Tippens§
Texas A&M University, College Station, Texas 77843

J. J. Jarmer and J. E. Simmons
Los Alamos National Laboratory, Los Alamos, New Mexico 87545

R. H. Jeppesen
University of Montana, Missoula, Montana 59812

G. E. Tripard
Washington State University, Pullman, Washington 99164
(Received 17 September 1987)

Angular distributions of the spin-correlation parameters A_{sl} and A_{ll} for the reaction $pp \rightarrow \pi^+ d$ have been measured at pion center-of-mass angles $40° \leq \theta^*_{\pi^+} \leq 130°$ at incident energies of 500, 650, and 800 MeV. Additional measurements of A_{ll} were made at 600, 700, and 750 MeV. The results of the experiment are compared with the predictions of several unified coupled-channel calculations and partial-wave analyses. While the latest partial-wave analyses were found to fit the data reasonably well, all except one of the various model predictions not only do not fit the data well, but also tend to be in disagreement with each other. The data show no clear sign of a need for proposed dibaryon resonances.

I. INTRODUCTION

Study of the nucleon-nucleon (NN) interaction, especially through single-pion production, plays an important role in our understanding of hadronic interactions. Furthermore, these studies shed light on the possible existence of the proposed[1,2] dibaryon resonances $^1D_2$ ($\sim$2140 MeV), $^3F_3$ ($\sim$2220 MeV), and $^1G_4$ ($\sim$2430 MeV). Although a substantial body of high-precision data have been accumulated on the unpolarized $pp \rightarrow d\pi^+$ differential cross section[3] and spin observables for the elastic channels, only in the last few years have more extensive spin-dependent measurements been made on the inelastic channels.[4–9] Because the predicted resonances are reported to have large inelasticity,[1] it is reasonable to expect that the inelastic single-pion production channel should be sensitive to these resonances. Furthermore, the spin observables should be more sensitive than the unpolarized differential cross section to such resonances.[2] In particular, the analyzing power and A_{sl}, being dependent on interference between triplet and singlet amplitudes, would be more likely to reveal the presence of dibaryon resonances.

Of the several inelastic single-pion production channels, the $pp \rightarrow \pi^+ d$ channel is most readily subjected to experimental and theoretical examination. The cross sections for the two-body $pp \rightarrow \pi^+ d$ and the three-body $pp \rightarrow pn\pi^+$ single-pion production channels are approximately the same at 500 MeV. The relative contribution from the $pp \rightarrow \pi^+ d$ channel steadily decreases as energy increases, but still accounts for about 5% of the single-pion production cross section at 800 MeV. Furthermore, because of the strong coupling which should exist between the two channels, the $pp \rightarrow \pi^+ d$ channel is expected to be influenced by most of the phenomena found in the dominant $pp \rightarrow np\pi^+$ channel. Finally, the $\pi^+ d$ final state is the simplest to study because it is a two-body final state in which both particles are charged.

For the $pp \rightarrow \pi^+ d$ channel most of the precision measurements made in the past have been of observables which can be investigated with an unpolarized target. In particular, the unpolarized differential cross section $\sigma_{00}(\theta)$[3] and the analyzing power $A_n(\theta)$,[5,6] have been studied from threshold up to 1.2 GeV. The recent availability of polarized target technology has made possible the measurement of observables such as the spin-correlation parameters. Some of the first experiments to measure the $pp \rightarrow \pi^+ d$ spin-correlation parameters were done by Aprile *et al.*[7] and Hoftiezer *et al.*[8] at the Schweizerisches Institute für Nuklearforschung (SIN). These measurements were all made at energies below 590 MeV, corresponding to invariant mass less than 2148 MeV and therefore span only a fraction of the energy region in which the proposed dibaryon resonances would

be found.

In this paper the first measurements of the $pp \to \pi^+ d$ spin-correlation parameters $A_{sl}(\theta)$ and $A_{ll}(\theta)$ above 582 MeV are reported in full, complementing an earlier partial report.[10] The results span the energy range 500–800 MeV, which corresponds to invariant mass 2112–2241 MeV, and complement earlier measurements of A_{nn} and A_n.[11] The data are compared with the predictions of two partial-wave analyses[12,13] and with the results of several calculations[14–17] based on unified coupled-channel theories of the $NN \to NN$, $\pi d \to \pi d$, and $NN \to \pi d$ reactions. In addition, the A_{sl} results are used to extend the A_{sl} versus A_n plots of Berdoz, Favier, and Foroughi[18] to 800 MeV.

II. FORMALISM

The reaction can be described following Foroughi[19] and Bourrely *et al.*[20] in terms of the helicity amplitudes, which are functions of deuteron helicity $\mu = 0, \pm 1$ and the proton helicities $\lambda_b, \lambda_t = \pm\frac{1}{2}$, where the subscripts b and t refer to the beam and target, respectively. The helicity amplitudes are a weighted sum over the singlet-triplet partial-wave amplitudes $a_0, a_1, \ldots, a_n$, defined by Mandl and Regge[21] and extended by Blankleider and Afnan.[14] They are listed in Table I for L_π up to 5. Also listed in this table are the relative angular momenta L_Δ between the nucleon and the $\Delta(1232)$ when the reaction proceeds through the N-Δ intermediate state. The entry * for L_Δ indicates that no intermediate N-Δ state is possible. Because of conservation of parity there are only six independent, complex helicity amplitudes M_1, T_2, T_3, M_4, S, and T_6, where the symbols S, T, and M were used by Foroughi[19] to indicate the initial-state singlet, triplet, and mixed nature of the amplitudes, respectively. The relationship between these amplitudes and the a_i were given by Bugg.[13] Since the initial-state particles are identical, Bourrely *et al.* using the formalism of Jacob and Wick[20] shows that S and T_6 are symmetric about $\theta^*_\pi = \pi/2$, that M_1 and M_4 are antisymmetric about $\theta^*_\pi = \pi/2$, and that $T_2(\theta) = -T_3(\pi - \theta)$. Thus at $\theta^*_\pi = \pi/2$, $M_i = 0$ and $T_2 = -T_3$.

The $\hat{l}, \hat{\mathbf{n}}, \hat{\mathbf{s}}$ coordinate system used here is defined in terms of $\hat{\mathbf{k}}_p$ and $\hat{\mathbf{k}}_\pi$, unit vectors in the laboratory directions of the incident proton and scattered pion, respectively,

$$\hat{l} = \hat{\mathbf{k}}_p \,, \tag{1a}$$

$$\hat{\mathbf{n}} = (\hat{\mathbf{k}}_p \times \hat{\mathbf{k}}_\pi)/|\hat{\mathbf{k}}_p \times \hat{\mathbf{k}}_\pi| \,, \tag{1b}$$

$$\hat{\mathbf{s}} = \hat{\mathbf{n}} \times \hat{l} \,. \tag{1c}$$

The spin-dependent differential cross section σ can be written in terms of the unpolarized cross-section σ_{00} and spin parameters A_{ij} as,

$$\sigma = \sigma_{00} \sum_{ij} P_i^b P_j^t A_{ij} \,, \tag{2}$$

where indices i and j indicate for the beam and target, respectively, the direction of the polarization ($i,j = s$, n, or l) or the lack of polarization ($i,j = 0$), P_i^b and P_j^t are the beam and target polarization components along the ith and jth direction, and the summation is over $i,j = 0, s, n$, and l. Furthermore, $P_0^b = P_0^t = A_{00} = 1$. For a target with pure longitudinal polarization, the cross section can be written in terms of the nonvanishing (parity conserving) spin parameters as

$$\sigma = \sigma_{00}(1 + P_n^b A_{n0} + P_s^b P_l^t A_{sl} + P_l^b P_l^t A_{ll}) \,. \tag{3}$$

The unpolarized differential cross section σ_{00} and spin parameters A_{ij} can be written as bilinear sums of the six complex helicity amplitudes. The expressions are

$$\sigma_{00} = \tfrac{1}{2}(|M_1|^2 + |T_2|^2 + |T_3|^2 + |M_4|^2 + |S|^2 + |T_6|^2) \,, \tag{4a}$$

$$A_{n0} = \frac{-1}{\sigma_{00}} \mathrm{Im}(M_4 T_2^* - M_1 T_3^* - S T_6^*) \,, \tag{4b}$$

$$A_{sl} = \frac{1}{\sigma_{00}} \mathrm{Re}(M_4 T_2^* - M_1 T_3^* - S T_6^*) \,, \tag{4c}$$

$$A_{ll} = \frac{1}{2\sigma_{00}}(-|M_1|^2 + |T_2|^2 + |T_3|^2 - |M_4|^2 - |S|^2 + |T_6|^2) \,, \tag{4d}$$

$$A_{nn} = -\frac{1}{\sigma_{00}}[\mathrm{Re}(T_2 T_3^* - M_1 M_4^*) + \tfrac{1}{2}|S|^2 + \tfrac{1}{2}|T_6|^2]$$

$$= -1 + \frac{1}{\sigma_{00}}(|M_t|^2 + |T_2 - T_3|^2) \,, \tag{4e}$$

where $M_t = M_1 + M_4$. These expressions reveal how some of the amplitudes can be determined if enough ob-

TABLE I. Notation for the partial-wave amplitudes.

Amplitude	pp state	L_{π^+}	L_Δ	Amplitude	pp state	L_{π^+}	L_Δ
a_0	$^1S_0$	1	*	a_8	$^1G_4$	3	2
a_1	$^3P_1$	0	1	a_9	$^3F_2$	4	1
a_2	$^1D_2$	1	0	a_{10}	$^3F_4$	4	3
a_3	$^3P_1$	2	1	a_{11}	$^3H_4$	4	3
a_4	$^3P_2$	2	1	a_{12}	$^3H_5$	4	3
a_5	$^3F_2$	2	1	a_{13}	$^1G_4$	5	2
a_6	$^3F_3$	2	1	a_{14}	$^1I_6$	5	4
a_7	$^1D_2$	3	0				

servables are measured. Because of the symmetry properties of the helicity amplitudes, σ_{00}, A_{ll}, and A_{nn} must be symmetric about $\theta_\pi^*=\pi/2$, although A_{n0} and A_{sl} need not be. Furthermore, the quantities

$$\sigma^T\equiv\sigma_{00}(1+A_{ll})=(|T_2|^2+|T_3|^2+|T_6|^2)\ , \quad (5)$$

$$\sigma^{SM}\equiv\sigma_{00}(1-A_{ll})=(|M_1|^2+|M_4|^2+|S|^2) \quad (6)$$

show that both the sum of the squares of the triplet and the sum of the squares of the mixed and singlet amplitudes can be measured directly. Finally, because of the antisymmetry of the M_i and the relationship $T_2(90°)=-T_3(90°)$, absolute values of the amplitudes S and T_6 and their relative phase Δ can be obtained at $\theta_\pi^*=90°$ when A_{sl}, A_{n0}, A_{nn}, and A_{ll} are all measured:

$$|S|^2=\sigma_{00}(90°)[1-A_{ll}(90°)]\ , \quad (7)$$

$$|T_3|^2=|T_2|^2=\tfrac{1}{2}\sigma_{00}(90°)[1+A_{nn}(90°)]\ , \quad (8)$$

$$|T_6|^2=\sigma_{00}[A_{ll}(90°)-A_{nn}(90°)]\ , \quad (9)$$

$$\Delta=\tan^{-1}\left[\frac{\mathrm{Im}(ST_6^*)}{\mathrm{Re}(ST_6^*)}\right]=\tan^{-1}\left[\frac{-A_{n0}}{A_{sl}}\right]\ . \quad (10)$$

In this paper the energy dependence of Δ at $\theta_\pi^*=90°$ is shown by a plot of A_{n0} versus $-A_{sl}$, and following Berdoz, Favier, and Foroughi,[18] the correlation between $A_{n0}/\sin(\theta_\pi^*)$ and $A_{sl}/\sin(\theta_\pi^*)$ at 800 MeV is also shown. Equations (7)–(9) were used in a previous paper[10] to determine the energy dependence of $|S|$, $|T_2|$, and $|T_6|$ at 90° from the data of the present experiment, and that result will not be reproduced here.

III. EXPERIMENTAL METHOD

The experiment was performed at the Clinton P. Anderson Meson Physics Facility (LAMPF) with a polarized proton beam and target. A sketch of the experimental setup is shown in Fig. 1 and is quite similar to the arrangement of Tippens *et al.*[11] The proton beam was polarized by a Lamb-shift ion source[22] that was capable of orienting the polarization vector in any desired direction. The direction of the polarization vector at the target could be determined to within ±3° through knowledge of its orientation at the source, and its precession through the beam-transport system. At incident proton energies of 500, 650, and 800 MeV, linear combinations of the spin observables A_{sl} and A_{ll} were measured with a beam having both longitudinal and transverse components of polarization. Two different mixtures of the components were used in order to make possible the separation of the two parameters. At 600, 700, and 750 MeV, only A_{ll} was measured, with a beam having purely longitudinal polarization. The absolute polarization of the beam could be measured to within ±2% by the quench ratio method.[23] An additional measurement of the transverse component of the beam polarization was provided by a polarimeter (POL) located about 2 m upstream of the polarized proton target (PPT). The polarimeter consisted of four pairs of scintillation counters located above and below, and to the left and right, to determine the transverse $\hat{\mathbf{s}}$ and $\hat{\mathbf{n}}$ components of the beam polarization by measurement of the asymmetry of protons scattered from a thin target ($\frac{1}{8}''$ CH_2). The polarimeter was calibrated to within ±0.5% against the beam polarization measured by the quench ratio method.[23] The sum of the counts in all of the scintillation counters of the polarimeter was also used as a secondary beam-intensity monitor. The primary beam-intensity monitor was an Ar-CO_2 ion chamber (IC) located about 1 m upstream of the PPT, which could be used to determine the relative beam intensities to better than 1.5%. The proton beam intensity used in this experiment was between 0.1 and 1.0 pA, and the beam polarization was 70–80%. The beam position was monitored with periodic exposures of polaroid film in the beam. Continuous monitoring was also done with the ratio of the rates in POL which were quite sensitive to beam movement. The beam size was ~0.5 cm horizontally and ~1.0 cm vertically.

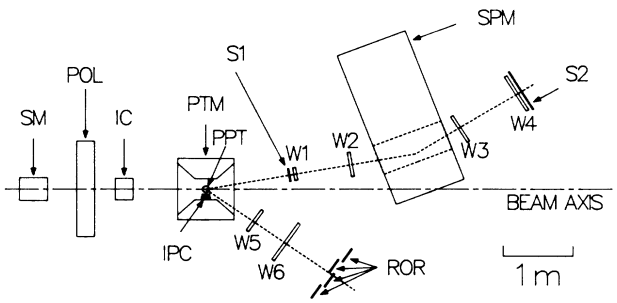

FIG. 1. Sketch of the experimental setup.

The longitudinally polarized proton target has been described previously;[24] it consisted of 2-mm diameter beads of frozen propanediol [$(CH_2)_3(OH)_2$] doped with 2% Cr^V by weight in a cylindrical container of length 5.5 cm and diameter 2 cm (17.3 cm^3), made of teflon of thickness 0.25 mm. The net free-hydrogen density of the target was 0.073 g/cm.[3] The target cell was immersed in a bath of liquid ^{3}He at a temperature less than 0.5 K and placed in a uniform (±0.01%) 2.5 T magnetic field produced by a pair of superconducting coils in the Helmholtz configuration. The coils of this PPT magnet (PTM) gave an unobstructed half-cone viewing angle of 45° with respect to the beam axis, limiting the angular range of pions detected outside the magnet to center-of-mass angles less than 80° (70° for 500 MeV). The field of the PTM caused the trajectories of scattered particles to be raised or lowered out of the horizontal plane containing the beam axis by an azimuthal angle $\Delta\phi$, as well as deflecting them toward the beam axis by a polar angle $\Delta\theta$. Since the incident proton beam traveled along the axis of the PTM (parallel to the magnetic field) its trajectory was unaffected. However, the field of the PTM precessed the transverse component of the incident beam polarization through angles of 30° to 40°, depending on the incident beam momentum. Compensation for a large fraction ($\frac{2}{3}$) of this precession was provided by a spin-precession magnet (SM) located about 2.5 m upstream of the target. The target material was polarized by the dynamic nuclear polarization method[25] using 71 GHz mi-

crowaves. The target polarization was 70–80 % and was monitored with a nuclear magnetic resonance (NMR) system[26] that read and recorded the NMR signal strength every two minutes during data acquisition. The system was calibrated to be reproducible to within ±4% about once a week by the thermal equilibrium method[11] at a temperature of 1 K. The absolute calibration was estimated to be ±5%.

A carbon target was also available to give an indication of the background contamination caused by the nuclei other than hydrogen in the target assembly. This carbon target consisted of a teflon cylinder identical to the propanediol container, filled with hollow graphite beads that yielded approximately the same net proton and neutron density as the oxygen and carbon in the propanediol target.

The deuteron and conjugate pion were detected in coincidence by a two-armed detector system (Fig. 1). Pions scattered at angles greater than 80° c.m. (70° for 500 MeV) were detected inside the bore of the PTM by a small (9×10 cm) scintillator (IPC). Pions scattered at angles less the 80° c.m. were detected outside the PTM by an external detector consisting of two multiwire x-y proportional chambers (MWPC's) $W5$ and $W6$ and a large scintillator array recoil or (ROR). The two MWPC's gave trajectory information which, when corrected for the deflection by the PTM, could be used to determine the polar and azimuthal angle of the pion at the target to within ±0.5°. These chambers were also used to obtain profiles of the reaction site within the target (target projections). The scintillator array provided the signal indicating an external pion event, as well as time-of-flight (TOF) and pulse height information. The entire external pion detector assembly was mounted on a movable cart that could be rotated about a point beneath the target center through laboratory angles from −15° to −45°. The cart could also be raised and tilted above the beam axis to accommodate the upward deflection of the pion trajectory out of the horizontal plane by the field of the PTM. The ROR array could also be raised to the height necessary to detect the pion after passage through $W5$ and $W6$.

The deuterons, over the entire angular range, were detected in a magnetic spectrometer (22° deflection angle) that included scintillators $S1$ and $S2$ and four x-y pairs of MWPC's $W1-W4$, two in front of and two behind the magnet (SPM). The scintillators measured the TOF over a 3.6-m flight path and the MWPC's were used to determine the momentum and scattering angle of the deuteron with resolutions of 2% (FWHM) and 0.5° (FWHM), respectively. Like the external pion detector the deuteron spectrometer was mounted on a platform that could be rotated about a point beneath the target center, through laboratory angles from 9° to 42°. Because of the size and weight of the spectrometer it was impractical to tilt it out of the horizontal plane to accommodate the deflection of the deuteron trajectory caused by the field of the PTM. Because of this constraint, the interaction plane was rotated out of the horizontal by a few degrees (6° to 10°) when deuterons had horizontal paths through the spectrometer. Compensation for this rotation of the interaction plane was achieved by a corresponding adjustment in the vertical location of the pion detectors. A π^+d event was triggered when there was a coincidence between the scintillators of the deuteron spectrometer and of the appropriate pion detector, provided that there were sufficient wire-chamber hits to reconstruct the event. The trigger required at least three out of four of both x and y planes be hit in $W1-W4$ and that there be hits in both x and y planes in either $W5$ or $W6$. These good π^+d events were written onto magnetic tape by the online PDP 11/60 computer.

Data were taken at six different beam energies and several different beam polarization orientations, which are listed in Table II. The actual kinetic energy of the incident beam was often a few MeV less than the nominal value. In addition the energy of the incident beam was reduced through energy loss by about 7 MeV as the beam passed through the cryostat and target material to the center of the target. The actual incident energies at the target center are listed in Table II. The uncertainty of the energy at the center of the target is estimated to be about ±4 MeV. In order to obtain the asymmetry, the direction of the beam polarization was periodically re-

TABLE II. Nominal energies used in the figures vs true incident proton energies at the target center, which take into account energy loss in the target.

Beam energy		Beam polarization
Nominal	True	orientation
500 MeV	488 MeV	Two different mixtures of longitudinally and transversely polarized beam.
600 MeV	589 MeV	Longitudinally polarized beam.
650 MeV	640 MeV	Two different mixtures of longitudinally and transversely polarized beam.
700 MeV	692 MeV	Longitudinally polarized beam.
750 MeV	743 MeV	Longitudinally polarized beam.
800 MeV	793 MeV	Two different mixtures of longitudinally and transversely polarized beam.

versed at the ion source. A reversal every two minutes helped to reduce systematic errors due to detector efficiency drifts. In addition, the target polarization was reversed by changing the microwave frequency. Data were acquired in cycles of four runs with two target reversals per cycle. The experiment was monitored and controlled through the computer, which was also used to perform a preliminary analysis on a sample of the data.

For both the on-line and off-line analyses, both the MWPC hit-position information and scintillator TOF were used to calculate a number of physical quantities which could be displayed as histograms, on which gates or cuts could be placed to reject invalid events. Information from the deuteron spectrometer was used to calculate the deuteron TOF, momentum, polar, and azimuthal c.m. scattering angles, missing mass, and to project the deuteron trajectories back to the target (deuteron target projections). If the external pion detector was used, the pion TOF, polar and azimuthal c.m. scattering angles, and target projections were also calculated. The combined information from both the external pion detector and the deuteron spectrometer gave the difference between the measured and expected pion c.m. angles and the deviation from coplanarity of the two trajectories. Histograms of these differences were later used to extract the yields associated with true π^+d events.

The data were analyzed off-line in several steps. The good π^+d events were first separated from the main body of data with a crude cut on the deuteron TOF. Also at this time, events with missing or multiple wire-hits in one of MWPC's were corrected by using information from the other wire chambers to estimate where the missing hit should have occurred, or to select the best choice in a multiple hit. The resultant subset of π^+d events was subjected to further cuts in order to reduce the background as much as possible. For external pion detector data, cuts were placed on the deuteron TOF, deuteron momentum, deuteron target projections, missing mass (with respect to the deuteron), the pion TOF, pion target projections, and coplanarity histograms. From data surviving these cuts, a histogram of the difference between the measured and the expected pion polar c.m. angles ($\Delta\theta_\pi^*$) was constructed. The $\Delta\theta_\pi^*$ histogram was subsequently fitted by a Gaussian peak superimposed upon a second-order polynomial. The polynomial was used to subtract the background underneath the peak in the $\Delta\theta_\pi^*$ histogram. For internal pion detector data, cuts placed on the histograms for the deuteron TOF, momentum, and target projections determined which data went into the missing mass histogram. The missing mass histogram was used to separate the background from the signal peak in the same manner as was done for $\Delta\theta_\pi^*$. These signal histograms are similar to the $\Delta\phi_\pi$ histogram appearing in Tippens *et al.*[11] The background for external pion data ranged from 3% to 10% while the background for internal pion data was considerably larger, in the 10–30% range, due to the absence of information about the pion kinematics. The accuracy of the background fits was verified by using the carbon target data. Since most of the background was expected to be the result of quasifree scattering from protons in the carbon and oxygen nuclei in the propanediol target material, the carbon data provided a good estimate of the size and shape of the background because the carbon contained approximately the same volume and density of bound protons as the propanediol. The fitted backgrounds were found to agree with the carbon target signal within a few (~ 5) percent. The data for each spectrometer setting were sorted into three center-of-mass angle bins, and the background-subtracted yields for each angle bin were normalized to the incident beam current and detector efficiency. The χ^2/ν value between different sets of equivalent data ranged between 0.01 and 2.

The asymmetries associated with these yields are a result of a combination of A_{n0}, A_{sl}, and A_{ll}. In general the use of Eq. (3) for a longitudinally polarized target and the relative yields from the four beam and target states gave four equations to solve for the three unknowns, σ_{00}, A_{n0}, and A_i', where

$$A_i' = (P_{is}^b A_{sl} + P_{il}^b A_{ll})$$

and i defines the polarization state. A χ^2-minimization technique was used to reduce the four equations to a set of three for each value of i. The problem could then be expressed in terms of three independent linear equations and three unknowns for each value of i. When the beam was purely longitudinal, $A_i' = P_{il}^b A_{ll}$. In general, however, the beam contained both longitudinal and transverse polarization components. Therefore two different beam polarization mixtures were needed; the two independent measurements A_1' and A_2' then gave two equations which could be solved for A_{sl} and A_{ll}.

IV. RESULTS AND DISCUSSION

The experimental values obtained for the two spin-correlation parameters A_{ll} and A_{sl} are given in Tables III and IV and are also plotted along with the predictions of two partial-waves analyses (PWA) (Refs. 12 and 13) in Figs. 2 and 4(a). The data are also compared with various model calculations in Figs. 3 and 4(b). Errors shown on the plots and given in the tables are purely statistical. The systematic error was due primarily to the uncertainty in the target polarization and the background subtraction in the case where $\theta_\pi^* > 80°$ (70° for 500 MeV). The error due to the background subtraction is in the worst case $\sim 5\%$ relative and when combined in quadrature with the uncertainty in the target polarization gives $\sim 7\%$ of the measured parameters. The c.m. angle bin width for each point is approximately 10°. There is fair agreement between values of $A_{ll}(\theta_\pi^*)$ measured by the external pion detector for $\theta_\pi^* \leq 80°$ and the complementary measurement for $\theta_\pi^* \geq 90°$ [i.e., $A_{ll}(\pi - \theta_\pi^*)$] by the inside pion counter. However, at 500 MeV the A_{ll} data are consistently higher for $\theta_\pi^* > 70°$.

A comparison of the data near 500 MeV with those of Aprile *et al.*[7] (SIN) is shown in Fig. 3 for A_{ll} and in Fig. 4(a) for A_{sl}, in which the SIN data are shown as crosses. The considerable disagreement between our data and the SIN A_{ll} results near 90° is not presently understood. One

major difference between the two experiments is that a magnetic spectrometer, which the SIN experiment lacked, was used in this experiment for momentum analysis of the scattered deuterons. In the analysis of our data, determination of the deuteron momentum was found to be essential in order to reduce the background in the region near 90°. Another difference is that in this experiment the background, principally due to quasifree scattering, was determined by least-squares fitting of a quadratic curve to the wings of the signal histograms, as explained in Sec. III; in the SIN experiment the background was determined only from carbon target measurements. It is interesting to note, however, that the SIN data near 90° are in much better agreement with the PWA of Hiroshige, Watari, and Yonezawa[12] and to a lesser extent with the PWA of Bugg.[13] The model calculations also seem to be in better agreement with the SIN measurement.

The recent PWA's of Hiroshige, Watari, and Yonezawa[12] and Bugg[13] make use of a large data set

TABLE III. Experimental values of A_{ll} vs $\theta^*_{\pi^+}$.

488 MeV		589 MeV		640 MeV	
A_{ll}	$\theta^*_{\pi^+}$	A_{ll}	θ_{π^+}	A_{ll}	$\theta^*_{\pi^+}$
−0.635±0.037	41.3	−0.457±0.020	39.7	−0.267±0.028	37.2
−0.597±0.040	49.9	−0.399±0.022	48.3	−0.291±0.029	40.9
−0.598±0.035	50.7	−0.376±0.020	49.6	−0.188±0.027	46.4
−0.568±0.035	54.9	−0.361±0.022	57.1	−0.222±0.040	50.0
−0.526±0.041	59.2	−0.336±0.027	57.3	−0.126±0.029	50.5
−0.618±0.036	60.2	−0.341±0.020	60.5	−0.225±0.027	55.5
−0.578±0.033	61.5	−0.359±0.028	63.7	−0.188±0.050	59.0
−0.628±0.042	68.2	−0.317±0.030	63.9	−0.145±0.039	59.3
−0.572±0.034	69.3	−0.317±0.022	67.4	−0.112±0.029	59.9
−0.446±0.034	92.4	−0.354±0.031	68.3	−0.129±0.056	63.4
−0.532±0.040	92.6	−0.332±0.028	71.0	−0.080±0.052	65.9
−0.518±0.031	93.8	−0.305±0.036	73.6	−0.110±0.060	68.6
−0.548±0.033	105.9	−0.369±0.033	73.9	−0.102±0.040	68.8
−0.494±0.031	106.9	−0.376±0.034	89.5	−0.079±0.053	73.2
−0.527±0.028	108.8	−0.290±0.033	103.2	−0.045±0.060	74.6
−0.532±0.034	116.1	−0.346±0.032	105.5	−0.030±0.028	82.0
−0.476±0.036	117.8	−0.298±0.030	117.9	−0.006±0.027	97.6
−0.495±0.031	119.4	−0.329±0.027	127.8	−0.090±0.027	110.3
692 MeV		743 MeV		793 MeV	
A_{ll}	$\theta^*_{\pi^+}$	A_{ll}	$\theta^*_{\pi^+}$	A_{ll}	$\theta^*_{\pi^+}$
−0.290±0.022	39.7	−0.330±0.025	36.3	−0.080±0.022	49.6
−0.151±0.022	48.8	−0.248±0.030	39.8	0.031±0.028	58.2
−0.141±0.022	49.6	−0.187±0.024	45.9	0.082±0.023	58.4
−0.095±0.023	57.6	−0.136±0.023	48.7	0.139±0.027	64.5
−0.066±0.025	57.9	−0.105±0.029	49.6	0.152±0.036	67.2
−0.027±0.021	60.3	−0.033±0.023	55.9	0.242±0.022	68.3
−0.044±0.032	63.8	0.008±0.023	57.9	0.243±0.037	71.4
0.001±0.025	64.6	0.009±0.026	58.2	0.277±0.026	72.3
0.029±0.022	67.9	0.019±0.029	60.4	0.304±0.039	76.7
0.031±0.032	68.5	0.045±0.032	64.1	0.401±0.043	83.4
0.052±0.026	72.5	0.092±0.027	64.9	0.413±0.049	96.4
0.080±0.031	74.1	0.135±0.024	68.1	0.354±0.042	103.1
0.155±0.040	86.3	0.157±0.034	68.9	0.336±0.045	107.8
0.132±0.037	94.1	0.205±0.027	72.4	0.241±0.037	114.7
0.122±0.039	100.2	0.217±0.033	74.5	0.062±0.033	123.9
0.137±0.032	103.6	0.243±0.026	83.4		
0.100±0.033	108.3	0.359±0.039	87.3		
−0.002±0.038	111.1	0.321±0.026	97.8		
0.094±0.029	111.9	0.257±0.037	102.1		
0.034±0.031	115.2	0.222±0.046	109.8		
−0.053±0.033	118.6	0.185±0.026	110.6		
−0.075±0.028	122.6	0.111±0.038	114.2		
−0.031±0.028	123.5	0.065±0.037	119.9		
−0.139±0.024	130.9	−0.022±0.033	127.4		

TABLE IV. Experimental values of A_{sl} vs $\theta^*_{\pi+}$.

488 MeV		640 MeV		793 MeV	
A_{sl}	$\theta^*_{\pi+}$	A_{sl}	$\theta^*_{\pi+}$	A_{sl}	$\theta^*_{\pi+}$
−0.475±0.031	41.3	−0.623±0.064	37.2	−0.836±0.026	49.6
−0.556±0.050	49.9	−0.670±0.049	40.9	−0.877±0.030	58.2
−0.475±0.030	50.7	−0.673±0.062	46.4	−0.844±0.028	58.4
−0.493±0.033	54.9	−0.742±0.050	50.0	−0.762±0.029	64.5
−0.530±0.052	59.2	−0.711±0.045	50.5	−0.806±0.039	67.2
−0.570±0.030	60.2	−0.717±0.056	55.5	−0.812±0.027	68.3
−0.577±0.033	61.5	−0.668±0.070	59.0	−0.759±0.040	71.4
−0.570±0.054	68.2	−0.728±0.046	59.3	−0.774±0.028	72.3
−0.566±0.034	69.3	−0.750±0.043	59.9	−0.765±0.043	76.7
−0.481±0.032	92.4	−0.793±0.064	63.4	−0.697±0.046	83.4
−0.367±0.033	92.6	−0.787±0.077	65.9	−0.739±0.046	96.4
−0.420±0.033	93.8	−0.841±0.069	68.6	−0.740±0.048	103.1
−0.382±0.029	105.9	−0.836±0.044	68.8	−0.689±0.042	107.8
−0.400±0.028	106.9	−0.746±0.075	73.2	−0.640±0.046	114.7
−0.416±0.027	108.8	−0.809±0.064	74.6	−0.580±0.041	123.9
−0.351±0.033	116.1	−0.790±0.028	82.0		
−0.395±0.032	117.8	−0.730±0.026	97.6		
−0.419±0.030	119.4	−0.654±0.026	110.3		

available since 1985 (Laptev and Strakovsky[27]) that has been supplemented by the addition of a considerable amount of spin-correlation data above 600 MeV, including the results of this experiment. In the analysis of Hiroshige, Watari, and Yonezawa[12] partial-wave amplitudes a_0 through a_8 were determined for energies from

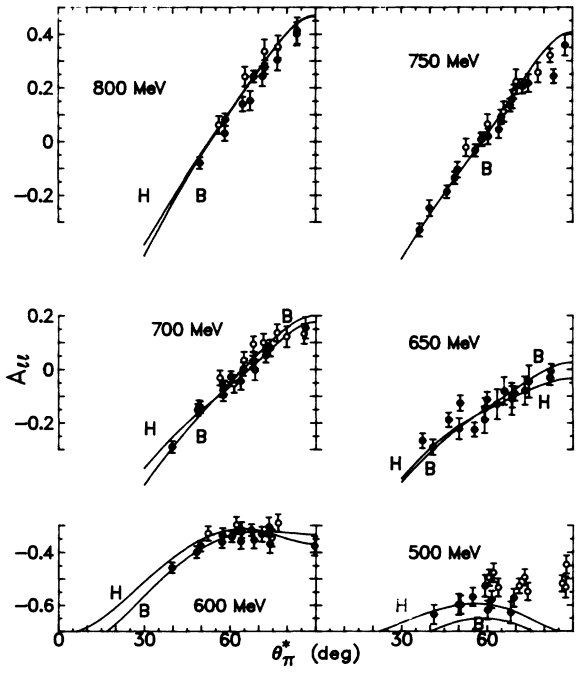

FIG. 2. Comparison of experimental A_{ll} data with partial-wave-analysis fits. The curves labeled H are from Hiroshige, Watari, and Yonezawa[12] and those labeled B are those of Bugg (Ref. 13). The open circles are data measured with $\theta^*_{\pi+} > 90°$ transformed by the symmetry relationship $A_{ll}(\theta) = A_{ll}(\pi - \theta)$.

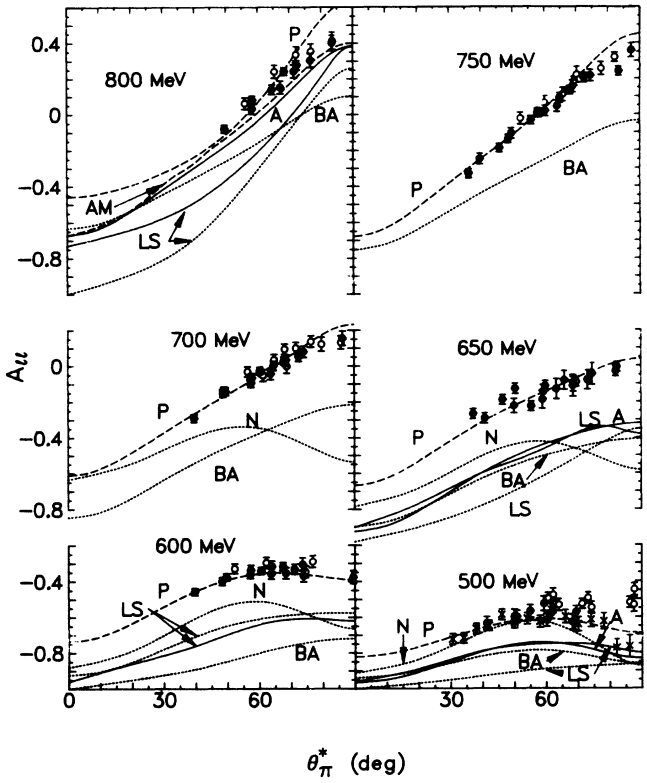

FIG. 3. Comparison of A_{ll} data with various model calculations. Labels are defined in the text. Solid lines are the calculations that used the present data; dashed lines are calculations with preliminary data from this experiment; dotted lines were obtained prior to the existence of these data. The crosses in the 500-MeV plot are the SIN results (Ref. 7). The open circles are as in Fig. 2.

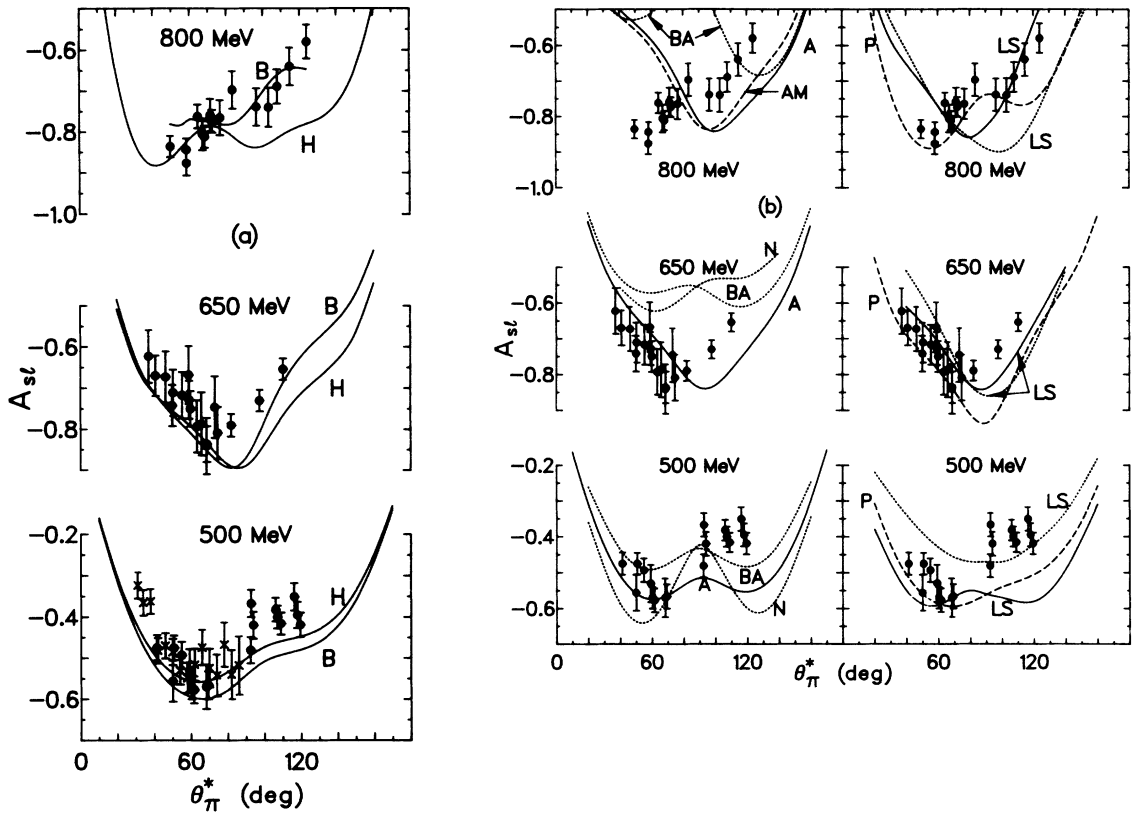

FIG. 4. (a) Comparison of A_{sl} with partial-wave-analysis fits labeled as in Fig. 2. The crosses in the 500-MeV plot are the SIN results (Ref. 7). (b) Comparison of A_{sl} with various model calculations, labeled as in Fig. 3 and the text.

threshold up to 810 MeV, and higher partial-waves were either taken from the theoretical predictions of Mizutani *et al.*[15] or set to zero. In his analysis Bugg[13] determined the partial-wave amplitudes a_0–a_6 (except for a_3) for the energy region 450–800 MeV, while he took a_3 and higher partial waves from Blankleider and Afnan[14] or set them to zero.

Except for the case of A_{ll} at 500 MeV near 90° these recent PWA's fit the data reasonably well. Both of these analyses predict large a_2 ($^1D_2$) and a_6 ($^3F_3$) amplitudes. It is argued by Bugg[13] and Niskanen[16] that the location of peaks in these amplitudes can be explained without the need to postulate dibaryons. The production of the $\Delta(1232)$ resonance near threshold in the vicinity of another nucleon makes possible low N-Δ orbitals in the intermediate state. Peaking would be expected in a_2 and a_6 at energies corresponding to the formation of N-Δ intermediate states with $L_\Delta=0$ and 1, respectively. If the deuteron had no binding energy, and hence no Fermi motion, the N-Δ intermediate states would be expected at pion lab energy $\sim$175 MeV, which corresponds to an incident proton lab energy of 637 MeV. Because the average momentum ($\sim$70 MeV/c) of the nucleons within the deuteron influences the kinematics of the interaction with the pion, these peaks will be shifted by amounts which depend upon L_Δ, the relative angular momentum of the spectator nucleon and the Δ. For $L_\Delta=0$ Bugg finds that the peak in the amplitude a_2 (corresponding to an N-N $^1D_2$ state) will be shifted downward by 67 MeV to $\sim$570 MeV, while the peak in the $L_\Delta=1$ amplitude a_6 (corresponding to an N-N $^3F_3$ state) is shifted upward by $\sim$20 MeV to 660 MeV. The fact that these amplitudes do peak near 570 and 660 MeV, respectively, is an indication that the interaction may be dominated by the expected threshold effects in Δ production in the intermediate state, although a dibaryon which could be a resonance between a nucleon and a Δ is not ruled out.

The predictions of Blankleider and Afnan[14] (BA), Locher and Svarc[15] (LS), Afnan and McLeod[16] (AM), Afnan[16] (A), Niskanen[16] (N), and Popping, *et. al*[17] (P) are shown along with the data for A_{ll} in Fig. 3 and for A_{sl} in Fig. 4(b). Blankleider, Afnan, and McLeod[14,16] use a set of coupled integral equations of the form of the Faddeev equations to describe simultaneously the NN→NN, NN→NNπ, and NN→πd channels. They preserve two- and three-body unitarity, perform an exact summation over all the pion multiple-scattering terms, and include varying degrees of relativistic corrections. The Locher and Svarc calculations do not preserve three-body unitarity, but include relativistic effects through a perturbation technique. Niskanen's coupled-channel calculations are nonrelativistic. Despite the agreement of these authors as to the basic ingredients of their calculations, there are still large differences among them as to how pion absorp-

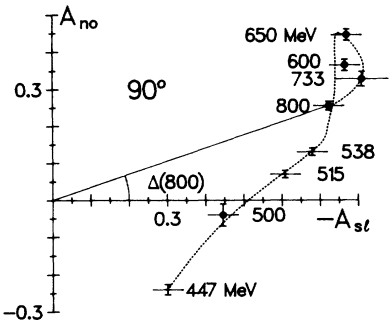

FIG. 5. Plot of $A_{n0}(90°)$ vs $A_{sl}(90°)$; solid points are the results of this experiment combined with Refs. 11 and 29; the remaining points are from Refs. 7 and 8. The dotted line is only a guide to the eye.

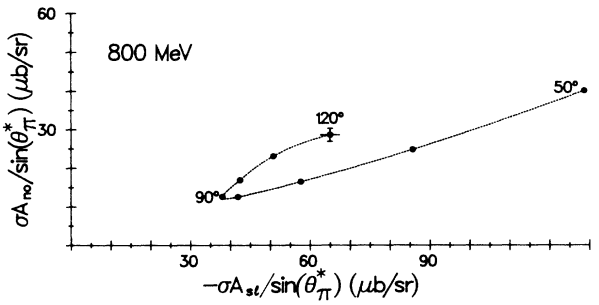

FIG. 6. Plot of $\sigma A_{n0}(\theta^*_{\pi^+})/\sin(\theta^*_{\pi^+})$ vs $\sigma A_{sl}(\theta^*_{\pi^+})/\sin(\theta^*_{\pi^+})$ at 800 MeV. The interval between points is 10°. The dotted line is only a guide to the eye.

tion should be taken into account and what the πN and NN scattering potentials should be. Heavy vector meson (ρ) exchange was included only in the calculations of Niskanen. Except for Popping, Sauer, and Xi-Zhang[17] none of the calculations are able to predict more than the general trend of the data. It is not clear at this stage what ingredients have been left out in these models and what accounts for the substantial differences between their predictions. A proper relativistic treatment of this problem is still not available.[28] It seems more sensible to resolve the differences between the predictions of these conventional models than to try to improve the agreement between any one of them and the data through the inclusion of features such as dibaryons or other six-quark states.

Other aspects of these spin-dependent parameters are shown in Figs. 5 and 6. In Fig. 5 data at 90° from Refs. 7, 8, and 11 are combined with the present A_{sl} results to exhibit the phase difference between the singlet S and the triplet T_6 amplitudes. The value of A_{sl} at 733 MeV is the result of a recent LAMPF experiment.[29] The phase at 800 MeV is shown by the angle $\Delta(800)$. The turnaround near 650 MeV is suggestive of some interesting dynamics in this energy region. Finally, in Fig. 6 following a suggestion by Berdoz, Favier, and Foroughi,[18] the correlation between the quantities $\sigma A_{n0}/\sin(\theta^*_\pi)$ and $\sigma A_{sl}/\sin(\theta^*_\pi)$ at 800 MeV is shown. It is intriguing that the resulting pattern is similar to the 542-MeV pattern of Berdoz, Favier, and Foroughi[18] except that the sequence of the points (0°→180°) is reversed, another indication that there may be dynamic changes occurring between 550 and 800 MeV.

V. CONCLUSIONS

New and more precise measurements of the $pp\rightarrow\pi^+d$ spin-correlation parameters A_{sl} and A_{ll} have been obtained in the 500 to 800 MeV energy range. With the exception of the 500 MeV A_{ll} measurement near 90° there seems to be no disagreement with data below 600 MeV which were previously available. As expected, partial-wave analyses which include the present results in their database give reasonable fits to the data. On the other hand, the coupled-channel predictions are found to do poorly in fitting the data and need to be improved before any conclusions can be drawn from them. The partial-wave analyses of Hiroshige, Watari and Yonezawa[12] and Bugg[13] have been much constrained by the inclusion of the new data. Their results do not call for the assumption of effects other than those expected from the dominance of the $pp\rightarrow d\pi^+$ reaction by the N-Δ intermediate states with $L_\Delta=0$ and 1. Results of the predictions based on different variants of unified models look promising, especially those of Popping, Sauer, and Xi-Zhang,[17] but the models need improvement before such exotic effects as dibaryon resonances should be built into them. It is anticipated that the contribution of the present experiment to the database will help resolve the question about the existence of these possible resonances with masses less than 2241 MeV when more complete inclusion of relativistic effects is accomplished, and the differences between the various model calculations are resolved.

ACKNOWLEDGMENTS

The mounting and execution of this experiment depended considerably on the operations staff and various support groups at LAMPF to whom we are very thankful. We are especially appreciative of Joe Vaninetti of the polarized target group. We would like to thank B. Blankleider, I. Afnan, and D. Bugg for enlightening discussions. We also thank them as well as N. Hiroshige and W. Watari for private communications of the effect of these data on their fits. Two of us (D.B.B. and R.H.J.) would also like to acknowledge support given to them by Associated Western Universities. This work was supported, in part, by the U. S. Department of Energy under Contract No. DE-AS05-76ER04449.

*Present address: University of California, Los Angeles, CA 90024.

†Present address: CEBAF, 1070 Jefferson Ave., Newport News, VA 23606.

‡Present address: Los Alamos National Laboratory, Los Alamos, NM 87545.

§Present address: University of Virginia, Charlottesville, VA 22901.

[1]N. Hoshizaki, Progr. Theor. Phys. **58**, 716 (1977); **60**, 1796 (1978).

[2]M. Roos *et al.*, Phys. Lett. **111B**, 1 (1982); R. R. Silbar, Comments Nucl. Part. Phys. **4**, 177 (1984).

[3]J. Boswell *et al.*, Phys. Rev. C **25**, 2540 (1982), and references contained therein.

[4]G. R. Smith *et al.*, Phys. Rev. C **30**, 980 (1984).

[5]G. Giles *et al.*, Phys. Rev. C **28**, 2551 (1983); A. Saha *et al.*, Phys. Rev. Lett. **51**, 759 (1983); H. Nann *et al.*, Phys. Lett. **88B**, 257 (1979).

[6]M. Corcoran *et al.*, Phys. Lett. **120B**, 309 (1983).

[7]E. Aprile *et al.*, Nucl. Phys. **A415**, 365 (1984); E. Aprile-Giboni *et al.*, *ibid.* **A415**, 391 (1984).

[8]J. Hoftiezer *et al.*, Nucl. Phys. **A412**, 273 (1984).

[9]T. S. Bhatia *et al.*, Phys. Rev. C **28**, 2071 (1983); R. Shypit *et al.*, Phys. Lett. **124B**, 314 (1983); C. L. Hollas *et al.*, Phys. Rev. Lett. **55**, 29 (1985); A. B. Wicklund *et al.*, Phys. Rev. D **35**, 2670 (1987).

[10]G. Glass *et al.*, Phys. Rev. C **31**, 288 (1985).

[11]G. Glass *et al.*, Phys. Rev. Lett. **53**, 1984 (1984); W. B. Tippens *et al.*, Phys. Rev. C **36**, 1413 (1987); W. B. Tippens, Ph.D. thesis, Texas A&M University and Los Alamos National Laboratory Report Nos. LA-9909-T, UC-34c, 1983.

[12]N. Hiroshige, W. Watari, and M. Yonezawa, Prog. Theor. Phys. **68**, 2074 (1982); **72**, 1146 (1984); private communication.

[13]D. Bugg, J. Phys. G **10**, 47 (1984); **10**, 717 (1984); D. V. Bugg, A. Hasan, and R. L. Shypit, Nucl. Phys. **A477**, 546 (1988); private communication.

[14]B. Blankleider and I. Afnan, Phys. Rev. C **24**, 1572 (1981); private communication.

[15]M. P. Locher and A. Svarc, J. Phys. G **11**, 183 (1985); T. Mizutani, C. Fayard, G. H. Lamot, and R. S. Nahabetian, Phys. Lett. **107B**, 177 (1981); private communication.

[16]I. R. Afnan and R. J. Mcleod, Phys. Rev. C **31**, 1821 (1985); I. R. Afnan (private communication); J. A. Niskanen, Nucl. Phys. **A298**, 417 (1978); Phys. Lett. **141B**, 301 (1984), and references therein.

[17]H. Popping, P. U. Sauer, and Zhang Xi-Zhan, Proceedings of VI International Symposium on Polarization Phenomenon in Nuclear Physics, Osaka, 1983 [J. Phys. Soc. Jpn. Suppl. **55**, 850 (1986)]; private communication.

[18]A. Berdoz, B. Favier, and F. Foroughi, J. Phys. G **10**, L71 (1984).

[19]F. Foroughi, J. Phys. G **8**, 1345 (1982).

[20]C. Bourrely, E. Leader, and J. Sofer, Phys. Rep. **59**, 95 (1980); M. Jacob and G. C. Wick, Ann. Phys. **7**, 404 (1959).

[21]F. Mandl and T. Regge, Phys. Rev. **99**, 1478 (1955).

[22]G. Ohlsen, LANL Report No. LA-4451, 1977 (unpublished).

[23]M. McNaughton *et al.*, Phys. Rev. C **23**, 1128 (1981).

[24]I. P. Auer *et al.*, Phys. Rev. D **29**, 2435 (1984).

[25]A. Abragam and M. Goldman, Rep. Prog. Phys. **41**, 395 (1978); V. A. Atsarkin, Usp. Fiz. Nauk. **126**, 3 (1978) [Sov. Phys. Usp. **21**, 725 (1978)].

[26]J. Boissevain and W. Tippens, LANL Report No. LA-9429-MS, 1983 (unpublished).

[27]A. B. Laptev and I. I. Strakovsky, Leningrad Nuclear Physics Institute reports, 1985 and 1986 (unpublished).

[28]H. Garcilazo, Phys. Rev. Lett. **53**, 652 (1984).

[29]R. L. Shypit *et al.*, Nucl. Phys. **A477**, 541 (1988).